Intercalated nanographite: Structure and electronic properties

B. L. V. Prasad, Hirohiko Sato, and Toshiaki Enoki*
Department of Chemistry, Tokyo Institute of Technology, 2-12-1, Ookayama, Meguro-ku, Tokyo 152-8551, Japan

Yoshihiro Hishiyama and Yutaka Kaburagi
Faculty of Engineering, Musashi Institute of Technology, 1-28-1, Tamazutsumi, Setagaya-ku, Tokyo 158-8557, Japan

A. M. Rao†
Department of Physics and Center for Applied Energy Research, University of Kentucky, Lexington, Kentucky 40506

Gamini U. Sumanasekera and P. C. Eklund
Department of Physics, Pennsylvania State University, University Park, Pennsylvania 16802-6300
(Received 23 October 2000; revised manuscript received 14 May 2001; published 15 November 2001)

Structural and electronic properties of K, Br_2, and I_2 intercalated nanographite compounds, prepared using standard intercalation techniques, were investigated. The staging phenomenon observed in bulk-graphite-intercalation compounds is absent in the case of intercalation compounds of nanographite, as expected for a finite-size host-guest system. K-intercalated samples contain a small fraction of potassium clusters apart from forming homogeneous mixtures of several stages. Many Raman features of K-intercalated nanographite were found to be similar to K-doped single-wall carbon nanotubes. The first evidence of charge transfer from nanographite to iodine, which is absent in bulk graphite, is revealed based on Raman scattering results. The charge transfer per carbon atom f_C follows the order potassium>bromine>iodine, which is similar to the trends observed in bulk-graphite-intercalation compounds. Intercalation of strong donors such as potassium makes the contribution of edge inherited nonbonding π states, which uniquely characterize pristine nanographite, less important. This is explained considering the large charge transfer and the accompanying shift of the Fermi level away from the edge states. In case of weak acceptors such as I_2, however, there is an enhancement in density of states that indicates a smaller shift in the Fermi level, keeping it in the vicinity of edge states.

DOI: 10.1103/PhysRevB.64.235407 PACS number(s): 68.65.−k, 71.20.Tx, 78.30.−j

I. INTRODUCTION

Carbon-based nanometer-scale materials have been a target of intensive studies recently.[1–7] Especially the reports that intercalation of electron donors and acceptors makes them good conductors and sometimes superconductors also have evoked a lot of interest in these systems.[8–10] Among several nanometer-scale sp^2-based carbon materials, fullerenes and nanotubes have been attracting greater attention. It has been found that during the preparation of fullerenes and nanotubes, several nanoscale graphite particles resembling onions are also formed.[4] However, studies on structures and electronic properties of these materials have been sparse owing to the difficulty in the preparation of particles with a homogeneous size distribution. In this connection, several recent reports have suggested that it is possible to prepare a large number of these polyhedral graphite particles with a highly homogeneous size distribution by heat treatment of diamond nanoparticles.[5–7] It is normally suggested that diamond (111) planes are quite unstable and can be converted to graphite (001) planes by heat treatment.[11] We have found that initial graphitization takes place on the surface at around 900 °C, and diamond is gradually converted to graphite from the surface inwards as the heat-treatment temperature (HTT) is increased,[6] the complete graphitization taking place at 1600 °C.[7] The prepared graphite nanoparticles at 1600 °C were found to have a polyhedral crystal habit with a hollow in the center, and the average size of the particle was about 7–8 nm. These graphite nanoparticles, which can be considered as an assembly of very weakly bound graphene nanosheets, make a good model system of nanographites. A hypothetical nanographene ribbon can be conceived as having only *trans*-polyacetylene-type zig-zag edge or *cis*-polyacetylene-type armchair edge. Theoretical calculations have shown that a nanographene ribbon with only zig-zag edges possesses edge inherited nonbonding edge states near the Fermi energy while an armchair edge does not give rise to such states.[12,13] It was also shown that for a graphene ribbon in general, even a few zig-zag edges per sequence are sufficient to show non-negligible edge states. In quite good agreement with the above-noted theoretical studies we have shown that there is significant enhancement of the electronic density of states around the Fermi energy in our graphite nanoparticles[6] due to localized nonbonding edge states. The edge states, which are unique to these materials, play quite a significant role in their electronic properties.[6,7] The difference in the electronic structure of nanometer-scale graphitic materials from bulk graphite is expected to impart novel features in their intercalated systems also. Iodine is known to form charge-transfer complexes with many polycyclic aromatic compounds including benzene,[14] while it does not form intercalation compounds with bulk graphite, which can be thought of as an infinitely extended network of benzene molecules. However, it was recently found that iodine forms charge-transfer intercalated compounds with single-wall carbon nanotubes[15] (SWNT's) as well as activated carbon

fibers[16] (ACF's), where the latter is characterized by a network of nanoscale graphite. Hence it would be interesting to study the effect of intercalation of both donors and acceptors, including iodine, into nanographite, to understand the similarity and difference in structure and electronic properties of these materials *vis-a-vis* bulk graphite.

In this paper we present the details of structure and electronic properties of intercalated nanographite where the nanographite itself was prepared from diamond nanoparticles by heat treatment at 1600 °C. We prepared graphite-intercalation compounds (GIC's) of potassium, bromine, and iodine with nanographite by employing the standard two-zone vapor-transport method.[17] Structural and electronic characteristics of these intercalated systems were analyzed on the basis of x-ray diffraction, Raman scattering, ESR, and magnetic susceptibility studies. It was found that the electronic properties of nanographite-intercalation compounds *vis-à-vis* bulk-graphite-intercalation compounds are crucially controlled by the charge-transfer rate to/from the nanosized π-electron system.

II. EXPERIMENT

The as-prepared nanodiamond particles (Cluster diamond, Tokyo Diamond Tool Mfg. Co.; grain size ~4–6 nm) are featured with transition-metal magnetic impurities, and HCl treatment is found to effectively remove these transition-metal impurities.[6,7] 20–50 mg of diamond nanoparticles boiled in HCl were placed in a graphite crucible and were heat-treated at 1600 °C under an inert Ar atmosphere for 3 h to obtain nanographite. Intercalation reactions with K, Br_2, and I_2 for the obtained nanographite were carried out by the standard two-zone vapor transport method used for the preparation of bulk GIC's.[17] Potassium-intercalated samples were prepared using the same conditions as those used for stage-1 K bulk GIC's except for ESR measurements. For ESR measurements two more samples with different potassium concentrations were prepared additionally using the procedures similar to stage-2 and stage-3 K bulk GIC's. The compositional ratios were estimated from the weight uptake measured under inert Ar atmosphere in a glove box. The compositional ratios reported here are averaged over several experimental observations.

X-ray diffraction was performed with a rotation-anode-type wide-angle x-ray diffractometer (Rad-rR RINT2000, Rigaku Co.) employing Cu $K\alpha$ radiation (50 kV, 300 mA) with a monochromator and scintillation counter. Intercalated compounds were mixed with Apiezon grease inside a glove box under Ar atmosphere for x-ray diffraction studies, thus avoiding any decomposition of the sample.

Raman spectra were measured in the backscattering configuration using a 514.5-nm Ar-laser excitation. The scattered light was analyzed in a Jobin Yvon HR460 single-grating spectrometer equipped with a charge-coupled array detector and a holographic notch filter (Kaiser Optical Systems, Inc.). 10–15 mg of the pristine sample was pressed into a hole at the center of Teflon or steel rectangular blocks. These blocks were then inserted into a rectangular Pyrex glass tube at one end, and at the other end the intercalate was kept in a breakable ampoule. The Raman spectra of the pristine sample were recorded first, and then the ampoule was broken. In case of K intercalation the potassium and nanographite zones were heated at 220 and 250 °C, respectively, while iodine intercalation was carried out by heating iodine and nanographite zones at 160 and 170 °C, respectively. Bromine is very volatile at ambient temperatures and hence Br_2 intercalation reaction was carried out at room temperature. However, after the intercalation reaction was over (usually in a matter of few minutes) excess bromine was removed by immersing the bromine zone in a liquid-nitrogen bath.

Magnetic susceptibility and magnetization were measured with Quantum Design MPMS-5 superconducting quantum-interference device (SQUID) susceptometer in the temperature range 2–300 K under magnetic fields up to 5 T. K-intercalated samples were transferred into a quartz glass tube inside a glove box and were sealed under vacuum. Br_2- and I_2-intercalation reactions were carried out in H-shaped glass tubes where one arm was joined to the quartz tube with nanographite and the other arm to a Pyrex glass tube containing Br_2 or I_2 inside a breakable ampoule. The whole chamber was sealed under vacuum and after breaking the ampoule intercalation reactions were carried out under conditions described as above. After the reaction was over the arm with Br_2 or I_2 was immersed in a liquid-nitrogen bath to drive out excess intercalate, and the quartz tube was sealed, enabling SQUID measurements to be carried out without exposing the intercalation product to outside atmosphere.

ESR spectra were measured with a conventional *X*-band spectrometer (JEOL JES-TE20), where the magnetic field and microwave frequency were calibrated using an NMR gaussmeter and a frequency counter, respectively. The K-intercalated samples were transferred to a quartz glass tube inside a glove box and were sealed under vacuum. For the I_2- and Br_2-intercalated samples ESR spectra were measured *in situ*, using similar procedures explained above for SQUID measurements. To obtain *g* values correctly we used diphenylpicrylhydrazyl (DPPH) as an internal standard.

III. RESULTS

Weight-uptake measurements indicated the composition of K-intercalated systems to be KC_9, KC_{29}, and KC_{36}, very close to those observed for stage-1, stage-2, and stage-3 bulk GIC's, respectively, when the same reaction conditions as those for the bulk K GIC's were employed. In this paper we have restricted our discussion mostly to KC_9 and compared it to bromine- and iodine-intercalated systems to make it clearer for discussion. Though the compositional ratio is very similar to that of stage-1 K-intercalated bulk graphite (KC_8), we did not observe any staging phenomenon for KC_9, as in bulk GIC's.[18] In order to clearly understand the origin of compositional similarity between stage-1 K bulk GIC's and KC_9 we have undertaken a detailed analysis of the powder x-ray diffraction of this compound. Figure 1 depicts the detailed powder diffraction pattern of both pristine nanographite and KC_9 around the 26° region. Diffraction in this region comes from the graphite (002) peak, which is largely affected by intercalation. We would like to point out that the

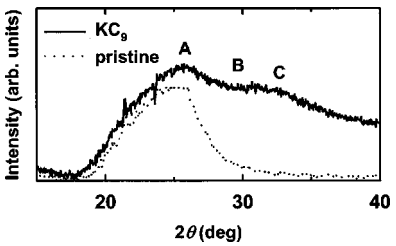

FIG. 1. The observed x-ray diffraction profiles in the vicinity of 26° for the pristine and KC_9 samples. *A*, *B*, and *C* denote the expected peak positions for nanographite (002), stage-2 (003), and stage-1 (002), respectively.

overall intensity of the x-ray diffraction is rather weak in the entire range observed (0°–90°) and we could observe a reasonable diffraction intensity only in this region with our instrument. As can clearly be seen in this figure the intercalated system retains the peak from pristine nanographite, a feature quite different from bulk GIC's. In bulk GIC's because of the staging phenomenon the *c*-axis repeat distance is quite different for each stage, that is, the (002) peak is observed at different locations, while the peak from the bulk graphite (002) diffraction around 26° is absent. Thus persistence of the graphite (002) peak even after K intercalation indicates that there is still some amount of unintercalated nanographite remaining. On the other hand, the small shoulders appearing around 29° and 33° clearly show the difference between intercalated and nonintercalated systems. It is worth noting here that the peaks at 29° and 33° correspond to the (003) diffraction peak of stage-2 and the (002) peak of stage-1 bulk GIC's, respectively, and they are the maximum intensity peaks in stage-2 and stage-1 systems.[19] To gain further knowledge, especially about the quantitative distribution of different stages in KC_9, the following analysis was undertaken. The observed x-ray intensities were first corrected for the Lorentz polarization factor and atomic scattering factor.[6] The atomic scattering factors for potassium and carbon were obtained from x-ray crystallographic tables,[20] and the scattering factor for the observed compositional ratio was estimated. Then the corrected profile could be fitted with three Lorentzian functions as depicted in Fig. 2 and the peak positions obtained were 25.4°, 29.1°, and 32.2°, corresponding

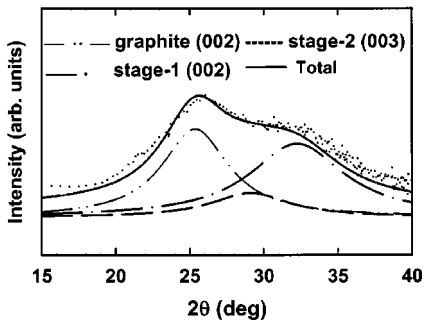

FIG. 2. The x-ray diffraction profile obtained after corrections for the Lorentz polarization factor and atomic scattering factor (see text for details). It was deconvoluted using contributions from pristine nanographite (002), stage-1 (002), and stage-2 (003).

to the graphite (002), stage-2 (003), and stage-1 (002) compounds, respectively.[19] Each peak intensity was further normalized for different *c*-axis repeat distances and different compositional ratios of pristine, stage-1, and stage-2 compounds enabling the calculation of corrected intensity A_C utilizing the equation

$$A_C = \frac{A}{[1+1/(F_K/nF_C)]/I_c}$$

where A is intensity from fitting, n is number of carbon atoms per intercalate in each stage (8 in stage 1 and 24 in stage 2), F_K and F_C are the atomic scattering factors of potassium and carbon, respectively,[20] and I_c is the *c*-axis repeat distance for the respective stage. The ratios of corrected intensities thus obtained correspond to the ratio of each component C, $CK_{1/8}$, and $CK_{1/24}$ in KC_9. We assumed that the difference in total weight uptake from the obtained ratios of different components and observed weight uptake corresponds to free neutral potassium atoms present in the sample. Thus from quantitative analysis of x-ray diffraction we could estimate that the total weight is made up of 36% of nonreacted carbon, 33% of $CK_{1/8}$, 26% of $CK_{1/24}$, and 5% of potassium clusters.

The compositional ratio for the Br_2- and I_2-intercalated systems, determined from weight-uptake measurements, was $C_{38}Br$ and $C_{65}I$, respectively. However, x-ray scattering for the I_2- and Br_2-intercalated samples was below the detection limit of our instrument, indicating an increase in the structural disorder in these samples. It is interesting to note here that similar observations were made on I_2-intercalated SWNT's.[15]

Raman scattering spectra of K-, Br_2-, and I_2-intercalated samples along with the pristine sample are provided in Fig. 3. The observed peaks were fitted with Lorentzian functions for the pristine and Br_2- and I_2-doped samples. For the K-intercalated sample a Breit-Wigner-Fano (BWF) function is employed for the peak around 1560 cm^{-1}, all other peaks being fitted with Lorentzian functions. The fitting parameters are provided in Table I. The pristine sample mainly shows three peaks at 1353, 1593, and 1623 cm^{-1}. The peak at 1593 cm^{-1} corresponds to the graphite E_{2g_2} mode, which is normally found upshifted from the bulk-graphite value of 1582 cm^{-1} in these finite-sized systems.[7] The peaks at 1352 and 1623 cm^{-1} are recognized to be originating from the disordered nature of these systems.[21] Doping of potassium clearly induces visible changes in the Raman spectrum. The E_{2g_2} mode is downshifted and displays a BWF line shape[22] given by

$$I(\omega) = I_0\{1+(\omega-\omega_0)/q\Gamma\}^2/\{1+(\omega-\omega_0)/\Gamma\}^2,$$

where $I(\omega)$ is the intensity as a function of frequency, I_0, ω_0, and Γ are the peak intensity, renormalized frequency, and full width at half maximum (FWHM) of the unweighted Lorentzian function (as $q\to\infty$ this equation represents a Lorentzian function). $1/q$ represents the interaction between the discrete E_{2g_2} mode and Raman-active continuum. From this analysis we find the peak position at 1566 cm^{-1} and $1/q = -0.32$. It is interesting to note that both the BWF peak

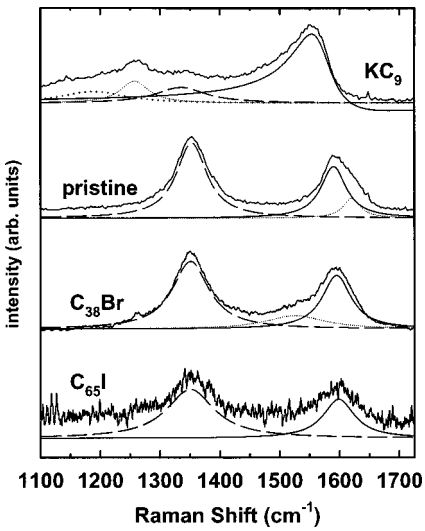

FIG. 3. Observed Raman spectra for the K-intercalated, pristine, Br_2-intercalated, and I_2-intercalated samples. The pristine, Br_2-intercalated, and I_2-intercalated samples were fitted with three, three, and two Lorentzian functions, respectively. For the K-intercalated sample, on the other hand, a BWF function and three Lorentzian functions were used. The fitting curves are also shown. The fitting curves were shifted down, where ever necessary, for clarity (see Table I for the fitting parameters).

position and the coupling parameter $(1/q)$ observed in the case of KC_9 are closer to those observed in K-doped SWNT's (Ref. 23) than bulk GIC's (Ref. 24). The other features of the Raman spectrum are also qualitatively more similar to those of K-doped SWNT's than bulk GIC's, the origin of which is not very clear yet. In case of Br_2- and I_2-intercalated systems the graphite E_{2g_2} mode is upshifted (1607 and 1603 cm^{-1}, respectively) by about 14 and 11 cm^{-1} compared to that found in pristine nanographite (Table I). We could also conclude that there are no adsorbed Br_2 or I_2 molecules in these intercalated samples, from the absence

TABLE I. Parameters for the Lorentzian and BWF functions used for fitting the observed Raman spectra. Note that the BWF function is used to fit the E_{2g_2} peak of KC_9.

Sample	Peak position (cm^{-1})	Peak width (cm^{-1})
Pristine	1352.9	30.8
	1592.7	25.7
	1623.2	17.1
KC_9	1187.9	65.0
	1257.4	29.1
	1334.8	50.9
	1566.1 (BWF)	39.4
Br_2 intercalated	1360.1	37.2
	1526.4	60.0
	1606.5	29.6
I_2 intercalated	1358.4	48.4
	1603.3	31.6

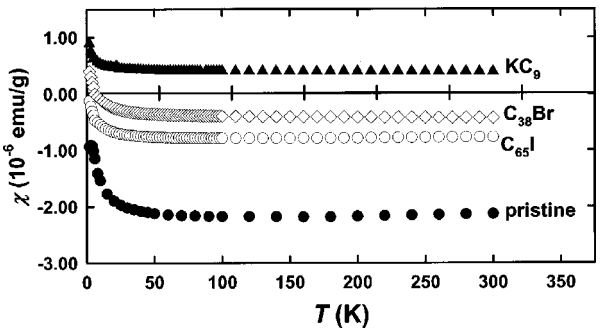

FIG. 4. The observed susceptibility for the pristine, $C_{65}I$, $C_{38}Br$, and KC_9 samples as a function of temperature under a magnetic field $H=1$ T.

of Raman peaks of neutral Br_2 or I_2. The origin of a small broad peak at 1526 cm^{-1} in the Br_2-intercalated sample is not very clear yet, but the presence of adsorbed Br_2 molecules can be ruled out because the higher harmonics of vibrational modes of Br_2 molecules do not fall in this range.[23] Thus the above-noted analysis clearly indicates that the graphite E_{2g_2} mode is found to downshift (upshift) when intercalated with donors (acceptors). This trend is very similar to that observed in bulk GIC's,[17] except that I_2 was not known to intercalate in bulk graphite. We have carried out Raman scattering analysis of the Br_2-intercalated product both in the presence of a large excess of Br_2 vapor in the cell and by driving out all the excess Br_2 by freezing the Br_2 zone in a liquid-N_2 bath. In both cases we found no appreciable difference in the E_{2g_2} peak shift, except that in the former case we could see very intense peaks corresponding to harmonics of vibrational modes of neutral Br_2 molecules. The similarity in the position of E_{2g_2} peak in both cases clearly suggests that the intercalation reaction is fairly irreversible.

The magnetic susceptibilities of all intercalated samples along with pristine sample are depicted in Fig. 4. The susceptibility of pristine sample is negative in the entire temperature range.[6] The absolute value at room temperature stays negative in iodine and bromine intercalation, showing a decreasing trend from iodine to bromine. The susceptibility becomes positive at low temperatures for the Br_2-intercalated system, while it is positive in the entire temperature range for the K-intercalated system. All the samples show a Curie-like rise at very low temperatures. The spin density, calculated from the Curie-like behavior, is about 0.2×10^{-3} spins/carbon atom in the pristine sample and decreases to $(0.1-0.08)\times10^{-3}$ spins/carbon atom after intercalation. The decrease in spin density after intercalation can be ascribed to the termination of localized defects or edge sites by formation of covalent bonds with the guest species. The value of χ_0 (susceptibility at $T=\infty$) is -26.6, -11.4, -6.1, and $+5.85$ (in units of 10^{-6} emu/mol of C atom) for the nonintercalated, iodine-, bromine-, and potassium-intercalated systems, respectively. This trend is directly controlled by the charge-transfer rate from/to the graphite π system as it becomes clear later.

The pristine nanographite shows an ESR linewidth of 3.5 mT and a g value of 2.0013 at room temperature, where the

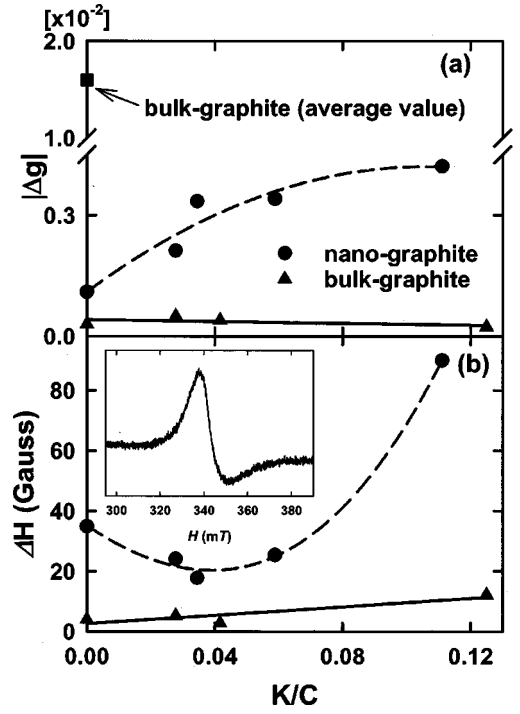

FIG. 5. (a) The g-value deviation ($|\Delta g|=|g_{\rm obs}-g_0|$), and (b) ΔH variations as a function of the K/C ratio for bulk and nanographite K-intercalated samples. The $g_\perp$ value for bulk graphite was used when comparing the deviations (for K/C=0) and the average g value $g_{\rm av}=(2g_\perp+g_\parallel)/3$ is also shown in the graph. Solid and dashed lines are only guides for the eye. The inset shows the room-temperature ESR spectral profile of KC_9.

g value is close to that of free-electron spin (g_0). All the potassium-intercalated nanographite samples show only one asymmetric ESR peak. A representative ESR spectra for the sample KC_9 is given as an inset in Fig. 5. As the intercalated potassium concentration increases the linewidths go through a minimum (~2 mT for KC_{29}) before becoming very broad for KC_9 (~9.5 mT) as can be seen from Fig. 5(b). The dependency of g values on the potassium concentration in bulk K GIC's is very small. They always stay in the vicinity of the free-electron spin value showing a linear dependency with a small negative slope as the potassium concentration increases.[25] In K-intercalated nanographite the dependency is quite pronounced with KC_9 showing the largest deviation ($g_{\rm obs}=1.9980$) as compared with the pristine nanographite, which is depicted in Fig. 5(a). This could be attributed to the enhanced spin-orbit coupling due to the specific sizes of these samples.[26] Br_2- and I_2-intercalated samples do not show any ESR signal.

The x-ray diffraction results, Raman spectra and compositional ratios could be interpreted in two ways; the results are either due to intercalation or just due to reaction on the surface of nanographites with the remaining core part unreacted. Because Raman analysis probes only the surface and x rays penetrate more deeply, it could be argued that the Raman results reveal a uniform phase formation whereas x-ray results show mixed-stage formation. However, the ESR results, where the microwave skin depth is larger than the particle size, suggest the homogeneity of the samples as mentioned above. Here, the interesting point to note is that the dependency of linewidths on potassium concentration is very similar in case of bulk GIC's and nanographite IC's.[25] The absence of an ESR signal in Br_2- and I_2-intercalated samples is again very similar to bulk-graphite systems. This is attributed to the charge transfer from the guest species to the nanographite and the resulting enhancement of spin-orbit coupling as explained for acceptor-intercalated bulk GIC's.[27] The similarity in the ESR behavior of bulk GIC's and nanographite intercalation compounds (IC's) clearly shows that uniform charge transfer between the nanographite and intercalate takes place in the bulk for all the nanographite IC's investigated. Other points worth noting here are the weight uptake and magnetic susceptibility. If the reactions only took place on the surface, then it is very difficult to understand the large weight uptakes as observed here. The susceptibility shows consistently larger upshifts upon intercalation than that of pristine nanographite as shown in Fig. 4. This cannot be explained by a simple summation of contributions from intercalated surface regions, nonintercalated interior regions, and nonreacted intercalate species on its surface. Hence it is proved unambiguously that the reactions observed here are intercalation reactions and not any *surface-only* phenomenon.

IV. DISCUSSION

Each particle of nanographite prepared at 1600 °C is found to have a polyhedral shape that is hollow inside.[6] The average particle size is about 7–8 nm, where each face of the polyhedron is made up of 3–7 graphene sheets.[6] If each of the nanographite particles is visualized as 3–6 closed polyhedral cages of different sizes contained in each other, it is difficult to comprehend the process of intercalation, since there is no way for the intercalates to access the graphene interplane galleries. However, these polyhedra are known to be formed by adjacent faces having open π-bond edges at the crossing point. Although participation of cross-linking bonds between adjacent graphene sheets may modify the features of the edges, a large number of them are expected to be left with open gaps due to termination of the edges by hydrogen or oxygen, since nanographite is treated in air. The presence of open edges enables the intercalate to access the interplane galleries of the graphene sheets to form the intercalation compounds. This makes the nature of the intercalation reaction different from that of fullerenes and carbon nanotubes having closed edges, where the dopants are present only in the interstitial sites.

X-ray characterization reveals the absence of staging phenomenon. The absence of staging phenomenon could be a direct consequence of the particle size, which is smaller than the correlation length of the density correlation function related to the staging transition, as the fluctuations overwhelm the energy gain due to the transition.[28] Moreover, for finite domain sizes, it is argued that the domination of entropy term leads to a form of stage disorder called ''random staging.''[29] In the present sample, which contains ''packages'' of intercalate and host that fluctuate in size, staging cannot be stabilized due to kinetic limitations in the interca-

lation process or imperfections in the host lattice. The *c*-axis repeat distances from the Bragg peak positions of stage-1 and -2 phases in these mixed stage systems were found to be 0.56 and 0.92 nm, respectively; about 4–5% higher than those observed for the same stages in the bulk K GIC's.[19] Owing to the turbostratic nature the *c*-axis repeat distance of pristine nanographite itself is about 5% higher than the bulk-graphite value, which explains the observed difference in the intercalated sample. Another interesting feature is the presence of neutral potassium clusters. At present it is difficult to pinpoint the location of these clusters in this sample. Two possible locations are the interstitial sites of the polyhedral cage (very similar to K-doped C_{60} and SWNT's where the K is present in the interstitial sites) or in the hollow present in each particle. Further studies such as high-resolution transmission electron microscopy are needed to answer this question, but the extreme air sensitivity of these samples is a big hurdle to overcome.

Iodine- and bromine-intercalated systems did not show any x-ray diffraction, although the experiments were carried out under conditions similar to those of potassium-intercalated compounds. The low charge-transfer rate generally associated with acceptor-intercalation systems results in a smaller interlayer interaction, which is known to contribute to the random stage ordering.[30] The low charge-transfer rate is also confirmed in the present iodine- and bromine-intercalated nanographites as we will show later. Therefore, in case of bromine and iodine intercalation we have more disordered systems compared to the K-intercalated systems. This leads to very weak scattering, well below the detection limit of our instrument.

Raman scattering has been an invaluable tool in analyzing the various forms of carbons as well as their doping products. Intercalation of donor or acceptor guests into graphite is accompanied by charge transfer. In case of donor intercalation, charge is transferred to the graphite π^* band resulting in an in-plane lattice expansion. As a consequence the graphite E_{2g_2} mode is found to be downshifted in addition to the BWF line shape observed. The origin of the BWF line shape, observed mainly for stage-1 alkali-metal-intercalation compounds, is explained as the interference of the discrete E_{2g_2} mode with a Raman-active continuum.[22] The continuum states are considered to arise from both in-plane and *c*-axis zone-folding effects owing to the lowering of symmetry, leading to a large number of Raman-active modes after intercalation.[24] It is somewhat surprising that we see only the BWF line shape characteristic of stage-1 formation while the x-ray study reveals that these compounds, in fact, are random-stage inhomogeneous compounds and are expected to show distinct Raman features corresponding to the graphite bound and interior layers. In the higher-stage bulk GIC Raman spectra, especially for third- and higher-stage compounds, two distinct peaks corresponding to the graphite bounding and interior layers having different amounts of charge transfer are seen.[17] However, in the third- and higher-stage bulk GIC's the graphite interior layers are almost completely screened from the bounding layers and have negligible charge transfer. In the present case due to random staging the charge transfer might be quite uniform among all the graphene layers, leading to the observation of only one peak, which is in good agreement with ESR results. The renormalized frequency from the BWF analysis in the case of KC_9 is found to be 1566 cm^{-1}, giving $\Delta w = 27\ cm^{-1}$ (Table I), where Δw is the difference in the Raman E_{2g_2} peak positions between the intercalated and pristine samples. The peak position observed here is somewhat higher than stage-1 alkali-metal bulk GIC's [1547 cm^{-1} (Ref. 24)] but very close to the K-doped SWNT's [1567 cm^{-1} (Ref. 23)]. It is generally found that the dependence of peak shift on the charge-transfer rate is linear in case of donors, and with use of the relation[31] between Δw and the charge-transfer rate per carbon atom, f_C, the charge-transfer rate is estimated at $f_C = 0.03$, which is about half of that for the bulk K GIC ($f_C = 0.075$).

The $1/q = -0.32$ we observe here has the same sign as bulk K GIC's (-1.2), but smaller in magnitude,[24] and again very close to that of K-doped SWNT's (-0.35).[23] The magnitude and sign of the $1/q$ value depict the strength of coupling and indicate whether the coupling is to a continuum of lower- (negative sign) or higher- (positive sign) frequency states. Thus the negative sign observed here indicates that the discrete E_{2g_2} phonon state is coupled to a Raman continuum of lower frequency vibrational states similar to bulk KC_8.[22] We also observed many modes in the range $\sim$1000–1300 cm^{-1}, similar to K-doped SWNT's. There may be two possible reasons for this. The SWNT's used for the intercalation reactions might contain a few nanosized graphite particles, similar to those studied here, and the intercalation of potassium into these nanoparticles might account for the similar features observed in these two independent studies. If that is the case the intensity of these mid-frequency peaks compared to the BWF line should be very less in the K-doped SWNT case, since the number of nanosized graphite particles compared to the SWNT's is considered to be very less (less than 10% by weight).[32] But we observed that the relative intensities of the BWF line and the mid-frequency modes in these two studies are quite similar. The other origin for the similar feature could be the size effects; since both these are finite-size systems, doping of potassium into them might lead to similar effects. It is shown that there are non-negligible density of vibrational states in the region 1100–1300 cm^{-1} for bulk graphite, which become Raman active at finite sizes due to the breakdown of wave-vector conservation.[21] In the present case also the significant Raman intensity in this region could be related to the breakdown of selection rules due to potassium doping in a random fashion. The similarities in the peak shifts, the $1/q$ values, and the observation of mid-frequency peaks are all in favor of the conclusion that both SWNT's and nanographite are featured with finite-size lattice networks, behaving in a similar way after potassium doping. This makes nanographite all the more interesting because from a structural point of view, these two are quite different from each other; the SWNT's are of a closed seamless cylindrical type, while nanographite is a weak assembly of finite-size flat graphene sheets with open edges. However, the clear

assignment of these mid-frequency peaks in both these cases must await further work.

Here, we consider the results of intercalation of acceptors into nanographite. As stated earlier, acceptor doping into graphite is accompanied by a charge transfer from the graphite π band to the acceptor molecules resulting in an upshift in the E_{2g_2} peak position.[17] For Br_2- and I_2-intercalated nanographite the peak positions are found to be upshifted by 14 and 11 cm^{-1}, respectively, indicating the stiffening of C-C bonds due to introduction of holes into the π band. In bulk GIC's, the Raman E_{2g_2} peak shift is directly related to the charge-transfer rate between the graphite π band and guest species. It was estimated based on Raman scattering studies during continuous electrochemical doping by H_2SO_4 that $\Delta w/f_C \approx +460\,cm^{-1}$ in acceptor GIC's, where Δw and f_C represent the peak shift and degree of charge transfer.[32] But, such a linear relation is not valid for weak acceptors like halogens, which are featured with very low f_C values.[33] Nevertheless, in the present case the peak shifts observed for acceptor nanographite IC's are generally higher than the corresponding peak shifts of bulk acceptor GIC's, and we assume that a linear relation between f_C and the peak shift is valid. This is partly justified by the fact that iodine, which does not form intercalation compounds with bulk graphite, does so with nanographite, proving that nanographite is a better donor than bulk graphite. Based on the value of $\Delta w/f_C$ given above and present Raman results, we find, for the Br_2 and I_2 samples, $f_C \approx 0.030$ and 0.024, equivalent to 1 hole per 33 and 42 carbon atoms, respectively. This is roughly comparable to the charge-transfer rate calculated on the basis of weight-uptake measurements $f_C \approx 0.026$ and 0.015 for Br_2 and I_2 intercalation, respectively, which is estimated on the assumption of a complete charge transfer and conversion of all intercalate molecules into Br^- or I^-. I_2 is not known to intercalate into bulk graphite; nevertheless, it is known to form charge-transfer complexes with small aromatic molecules such as perylene.[14] The small aromatic molecules and infinite-sized bulk graphite can be taken as examples of two extremes of the conjugated π-electron system. According to the results on ACF's there seems to be a threshold limit of 6 nm for the in-plane size, above which iodine cannot react with the conjugated π-electron systems.[16] In the present case the average in-plane size of the graphene sheet is around 4 nm, thereby allowing a moderate charge transfer from the graphite π band to iodine. SWNT's also form intercalation compounds with I_2, displaying a moderate charge transfer of 0.018, leading to the formation of I_3^- and I_5^- species in the interstitial channels of the SWNT bundle.[15] In ACF's, with many neutral I_2 molecules present in the micropores, the charge-transfer rate is reported to be 0.008.[16] The roughly similar charge-transfer rates with iodine thus suggest that these three mesoscopic systems have a similar affinity towards iodine. Nanographites are featured with several defects as well as open π-bond edges. It is normally proposed that the intercalation is nucleated at the edges or defect locations in the graphite network, slowly encompassing the whole graphite network. The nanographite studied in the present case possesses large fractions of edge sites and defects, favorable for intercalation even for weak acceptors such as I_2. Here, it should be noted that for $C_{38}Br$ and $C_{65}I$ the charge-transfer rate f_C from both the Raman shift of the E_{2g_2} mode and the compositional ratios are overestimated due to the oversimplified assumption in the Δw-vs-f_C relation and the formation of covalent bonds as described below. Alternative procedures are necessary for these two cases for obtaining convincing f_C's and are discussed in the subsequent paragraphs.

Another interesting feature of acceptor-intercalated nanographites is irreversibility. In case of bulk Br_2 GIC's, about 30% of Br_2 uptake at saturation seems to be retained when the Br_2 vapor pressure is below a threshold limit, forming a ''residue'' compound.[17] The formation of the residue compound is ascribed to trapping of Br_2 molecules at the in-plane imperfections (stacking faults and dislocations). Br_2-intercalated SWNT's show a fairly reversible nature,[23] where deintercalation is achieved by simply reducing the Br_2 vapor pressure in the cell. However, I_2-intercalated SWNT's have to be heated to high temperatures of 250 °C for deintercalation.[15] In the case of Br_2 nanographite IC's, simply decreasing the Br_2 vapor pressure in the cell does not lead to deintercalation. Since nanographites are characterized with many defects and open edges, it is possible that intercalate molecules are trapped at these places, leading to the irreversible nature of intercalation reaction. From ESR results we could confirm that both Br_2 and I_2 could be partially driven out from the nanographite IC's by heat-treating them above 150 °C.[26] The localized spin-density estimations clearly reveal a decreasing trend with intercalation [0.2×10^{-3} spins/carbon atom in pristine sample, and $(0.1-0.08)\times10^{-3}$ spins/carbon atom after intercalation]. From the spin-density estimations we can conclude that some of the guest species have formed covalent bonds with defect sites. The partial deintercalation could be due to inadequacy of this heat treatment to remove covalently bonded bromine and iodine species.

We next discuss the consequences of charge transfer on the electronic structure of nanographite based on magnetic susceptibility studies. In Fig. 6 we provide the changes in $\chi_0-\chi_{core}$, where χ_{core} is the core diamagnetism estimated from Pascal's rule, as a function of the absolute value of the Raman E_{2g_2} peak shift. The Raman E_{2g_2} peak shift is known to be crucially controlled by the charge-transfer rate per carbon atom, f_C.[32,33] $\chi_0-\chi_{core}$ has contributions from the orbital susceptibility χ_{orb} and Pauli susceptibility $\chi_{Pauli,}$ where χ_{orb} is due to the itinerant motion of conduction carriers and χ_{Pauli} is related to the density of states at Fermi level. $\chi_0-\chi_{core}$ is negative for the pristine nanographite. From the figure it is clear that as the peak shift increases the absolute value of $\chi_0-\chi_{core}$ decreases from pristine through the bromine-intercalated sample, and $\chi_0-\chi_{core}$ finally becomes positive in KC_9. This is directly related to the charge-transfer rate from/to the guest species, a scenario similar to bulk GIC's. In bulk acceptor GIC's the charge transfer is low and the orbital susceptibility remains diamagnetic.[17] On the other hand, the charge-transfer rate for KC_8 is very high and the orbital susceptibility is paramagnetic.[17] In other words, the

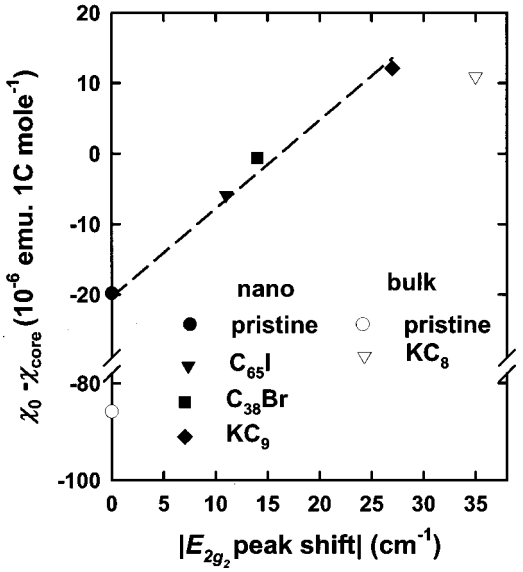

FIG. 6. The variation of $\chi_0 - \chi_{\text{core}}$ as a function of absolute value of Raman E_{2g_2} peak shift. The peak shifts for bulk-graphite samples are shown with respect to 1582 cm^{-1} (E_{2g_2} peak position of bulk graphite) and those of nanographite samples are with respect to 1593 cm^{-1} (E_{2g_2} peak position of pristine nanographite). The line is only a guide to the eye.

Fermi level in bulk acceptor GIC's is very close to the π-π^* contact point, while in KC_8 it is shifted away from it. The large diamagnetic susceptibility in bulk graphite is attributed to the interband transitions due to the overlap of π and π^* bands at the K point of the Brillouin zone where the Fermi energy is located.[34] However in bulk KC_8 the Fermi energy is shifted $\sim$1 eV higher than the Fermi level of pristine graphite as a consequence of charge transfer from the potassium 4s level to the graphite π^* band. This means that the interband transition between the π and π^* bands does not contribute to the orbital susceptibility; instead it comes from the intraband transition.[35] For pristine nanographite also we found that the susceptibility is negative in the entire temperature range investigated, in which orbital diamagnetism (χ_{orb}), plays an important role.[6] In addition we proved that the Pauli susceptibility in pristine nanographite is enhanced almost by two orders of magnitude,[6] good evidence for the presence of edge inherited non-bonding π states near the Fermi energy as predicted by many theoretical studies.[12,13] In the case of KC_9 the susceptibility becomes positive in the entire range, in sharp contrast to the behavior of pristine sample (Fig. 4). From x-ray analysis we found that KC_9 is in fact a mixed-phase inhomogeneous compound. In a preliminary report earlier we have shown that the total susceptibility observed at room temperature could be accounted for as the algebraic sum of the susceptibilities of individual components of KC_9, multiplied by their respective fractions, obtained from x-ray analysis.[18]

This analysis is based on two assumptions: (i) the presence of inhomogeneous charge transfer to graphite and (ii) the several stages formed are quite independent from each other. But as stated earlier the formation of inhomogeneous or rather random staging is a consequence of the nanometer-size host-guest system, and the several stages formed might have appreciable interactions with each other. Hence we can easily expect that the charge transfer is quite uniform among all the graphene layers. The observation of only one Raman peak around the E_{2g_2} region and the ESR results also support this contention. Thus we need a more comprehensive analysis of the magnetic susceptibility.

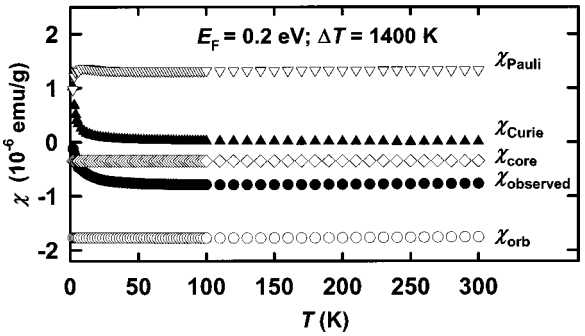

FIG. 7. Detailed susceptibility analysis for $C_{65}I$ based on the Kotosonov equation (Ref. 36) for disordered graphite. See text for details.

Here in order to get a rough quantitative estimate of χ_{Pauli} for all the nanographite-intercalated systems, with the new protocol of uniform charge transfer, we adopt the following two procedures. The χ_{orb} of bulk K and Br_2 GIC's are known to crucially depend on the compositional ratio, and we assume that the χ_{orb} for KC_9 and $C_{38}Br$ are the same as that of bulk K (Ref. 36) and Br_2 GIC's (Ref. 37) with similar compositional ratios. Then, using the equation $\chi_0 - \chi_{\text{core}} = \frac{1}{3}\chi_{\text{orb}} + \chi_{\text{Pauli}}$ and with the $\chi_0 - \chi_{\text{core}}$ values obtained, we can calculate χ_{Pauli} for KC_9 and $C_{38}Br$, where the factor $\frac{1}{3}$ in the first term is associated with the directional average for powdered samples. For $C_{65}I$, however, we cannot follow similar procedures since bulk graphite does not form intercalation compounds with iodine. However, the observed susceptibility of I_2-intercalated system displays a small temperature dependence around room temperature, similar to pristine nanographite,[6] suggesting that the Fermi level is very close to the π-π^* degeneracy point. Hence in this case we could carry out a detailed analysis (Fig. 7) of the susceptibility as carried out for pristine nanographite,[6] based on the Kotosonov equation[38] for disordered graphite,

$$\chi_{\text{orb}}(10^{-6}\ \text{emu/g}) = -\frac{4.6\times 10^{-3}\ \text{sech}^2\{E_E/2k_B(T+\Delta T)\}}{T+\Delta T},$$

where E_F is the Fermi energy and ΔT is the degeneracy temperature representing the energy level broadening due to randomness. The estimated values of the Fermi energy and degeneracy temperature from this analysis are 0.2 eV and 1400 K, respectively. The small change in E_F compared to pristine nanographite ($E_F \sim 0.1$ eV) is clearly in accordance with small charge transfer. In fact, here we can estimate the f_C's for $C_{38}Br$ and $C_{65}I$ using the equation[39]

$$f_C = \frac{1}{\sqrt{3}\pi\gamma_0^2}[E_F(I)^2 - E_F(P)^2],$$

TABLE II. Comparative values of χ_{orb} (directionally averaged value) and χ_{Pauli} for nanographite and their intercalated compounds. Comparative values for bulk graphite and KC_8 are also shown.

	χ_{orb} (10^{-6} emu/mol of C atom)	χ_{Pauli} (10^{-6} emu/mol of C atom)
Bulk graphite	-86[a]	0.2[b]
Nanographite	-40.2[c]	20.4[c]
$C_{65}I$ (from nanographite)	-24.3	19.2
$C_{38}Br$ (from nanographite)	-1.4[d]	0.8
KC_9 (from nanographite)	7.8[e]	5
KC_8 (from bulk graphite)	5.9[f]	5[f]

[a]Reference 42.
[b]Reference 43.
[c]Reference 6.
[d]Calculated from the extrapolated values of Ref. 37.
[e]Calculated from the extrapolated values of Ref. 36.
[f]Reference 36.

where γ_0 is 3.12 eV and $E_F(I)$ and $E_F(P)$ are Fermi energies of intercalated and pristine systems, respectively. The Fermi energy of $C_{38}Br$ is estimated through χ_{Pauli} from Ref. 40 and that of $C_{65}I$ was obtained from the fitting of the Kotosonov[38] equation (Fig. 7), discussed above. In Table II we provide the comparative values of χ_{orb} and χ_{Pauli} for bulk graphite and nanographite and their intercalated systems. Table III displays the charge-transfer rates for the nanographite IC's investigated here. From Table III it is clearly proved that the charge-transfer rate is in the order of $f_C(\text{potassium}) > f_C(\text{bromine}) > f_C(\text{iodine})$, which is similar to the trends observed in bulk GIC's,[17] although there is an interesting difference from the bulk GIC's. Namely, the charge-transfer rate for donor nanographite IC's is lower than that of bulk counterparts ($f_C = 0.03$ for K nanographite IC and $f_C = 0.075$ for bulk K GIC), whereas the formation of I nanographite IC's suggests the enhancement of charge transfer for acceptor nanographite IC.

Table II provides very important information regarding the electronic structure of these systems. It is clear that the χ_{Pauli}'s of bulk KC_8 and nanographite KC_9 are same and the enhancement observed in the case of pristine nanographite in comparison with bulk graphite is absent. In KC_8 from bulk graphite the large density of electronic states at E_F due to the three-dimensional (3D) interlayer-intercalate states causes the enhancement of Pauli susceptibility when compared to pristine bulk graphite.[41] Pristine nanographite, on the other hand, shows a large enhancement in Pauli susceptibility that is attributed to the edge inherited nonbonding states.[6] After K intercalation, however, the Pauli susceptibility decreases and becomes very similar to that of bulk KC_8. This clearly proves that the electronic structures of nanographite KC_9 and bulk KC_8 are similar to each other. The electronic structures of pristine bulk and nanographite mainly differ at the zero gap point, where the Fermi energy and the edge inherited nonbonding π states are located. However, charge transfer due to the intercalation of donor atoms such as potassium shifts the Fermi energy away from the zero gap point, making the electronic structure of nanographite and bulk graphite quite similar to each other; where they can be characterized with a combination of the 2D π band and the 3D interlayer-intercalate band.[41]

TABLE III. The charge-transfer rates per carbon atom determined for the three intercalates studied here. Different procedures were adopted to calculate these values and the details are provided in the text.

	f_C
KC_9	0.03
$C_{38}Br$	0.001
$C_{65}I$	0.0005

In Br_2- and I_2-intercalated nanographites, on the other hand, the charge-transfer rate is very low and hence the Fermi energy is still very close to the π-π^* contact point. The striking point here is the survival of the large Pauli susceptibility in the iodine-intercalated sample. Since iodine is known to be a very weak acceptor, we cannot relate this large Pauli susceptibility to the intercalate-interlayer band as we did for potassium intercalation.[41] Alternatively, the small shift in Fermi energy readily provides an explanation for the large Pauli susceptibility observed here. Many theoretical studies[12,13] as well as experimental investigations[6,7] have already proved that the nanographites are featured with edge inherited nonbonding states around the Fermi energy. Though theoretical reports suggest that the nonbonding π states from the edges appear as a flat band near the contact point of the π-π^* levels, the disordered structure of the present samples would induce an energy-level broadening. Therefore, it is clear that near the Fermi level of $C_{65}I$, there is an appreciable presence of nonbonding edge states and hence the enhancement in Pauli susceptibility.

V. CONCLUSIONS

Investigation of structural and electronic characteristics of intercalated nanographite, which itself was prepared from the heat treatment of diamond nanoparticles, is reported. The reaction procedures used for the preparation of bulk-graphite-intercalation compounds are found to be working even for nanographite. The staging phenomenon observed in bulk-graphite-intercalation compounds is absent in the nanographite-intercalation systems, owing to the geometry of the particles and the nanoscale size, where the correlation length of the density correlation function related to the staging transition will be larger than the particle size. Potassium-intercalated systems also indicated the presence of potassium clusters along with random stage systems. The vibrational characteristics of intercalated nanographite were very similar to the vibrational properties of doped single-wall carbon nanotubes rather than intercalated bulk graphite. The nanometer-size π system and many defects are considered to play a major role in accepting I_2 as an intercalate in these systems. The absence of complete reversibility of intercalation reaction even at elevated temperatures is ascribed to the

formation of covalent bonds between the guest species and the defect sites or edge sites. With K and Br_2, which are a relatively stronger donor and acceptor than I_2, respectively, the charge transfer is appreciable, shifting the Fermi level away from the π-π^* contact point and leading to an electronic structure similar to that of bulk GIC's. It is clearly proved that iodine forms charge-transfer complexes with nanographite systems unlike bulk graphite. However, the charge-transfer rate is very low, leading to a small shift in the Fermi energy, thus keeping the Fermi level in the vicinity of edge inherited nonbonding π states, leading to an enhancement in density of states.

In summary, the present investigations confirm that the structure and electronic properties of the intercalated nanographites are crucially determined by their size and the charge-donating/accepting capacity of the guest species. They also reveal that iodine forms nanographite intercalation compounds with a feature quite unique to nanographites and other nanosized π-electron networks.

ACKNOWLEDGMENTS

The present work was supported by the Grand-in-Aid for ''Research for the Future Program,'' Nano-carbons, from JSPS. A.M.R. and P.C.E. would also like to acknowledge financial support from the MRSEC NSF Grant No. DMR 9809686.

*Author to whom correspondence should be addressed. E-mail address: tenoki@chem.titech.ac.jp

†Present address: Department of Physics and Astronomy, Clemson University, 107 Kinard Laboratory of Physics, Clemson, SC 29634-0978.

[1] M. S. Dresselhaus, G. Dresselhaus, and P. C. Eklund, *Science of Fullerenes and Carbon Nanotubes* (Academic, San Diego, 1996).

[2] S. J. Tans, M. H. Devoret, H. Dai, A. Thess, R. E. Smalley, L. J. Geerligs, and C. Dekker, Nature (London) **386**, 474 (1997).

[3] J. W. G. Wildoer, L. C. Venema, A. G. Rinzler, R. E. Smalley, and C. Dekker, Nature (London) **391**, 59 (1998).

[4] D. Ugarte, Nature (London) **359**, 707 (1992).

[5] V. L. Kuznetsov, A. L. Chuvilin, E. M. Moroz, V. N. Kolomiichuk, Sh. K. Shaikhutdinov, and Yu. V. Butenko, Carbon **32**, 873 (1994).

[6] O. E. Andersson, B. L. V. Prasad, H. Sato, T. Enoki, Y. Hishiyama, Y. Kaburagi, M. Yoshikawa, and S. Bandow, Phys. Rev. B **58**, 16 387 (1998).

[7] B. L. V. Prasad, H. Sato, T. Enoki, Y. Hishiyama, Y. Kaburagi, A. M. Rao, P. C. Eklund, K. Oshida, and M. Endo, Phys. Rev. B **62**, 11 209 (2000).

[8] R. S. Lee, H. J. Kim, J. E. Fischer, A. Thess, and R. E. Smalley, Nature (London) **388**, 255 (1997).

[9] M. J. Rosseinsky, J. Mater. Chem. **5**, 1497 (1995).

[10] K. Tanigaki, S. Kuroshima, J. Fujita, and T. W. Ebbesen, Appl. Phys. Lett. **63**, 2351 (1993).

[11] V. L. Kuznetsov, I. L. Zilberberg, Y. V. Butenko, A. L. Chuvlin, and B. Segall, J. Appl. Phys. **86**, 863 (1999).

[12] K. Nakada, M. Fujita, G. Dresselhaus, and M. S. Dresselhaus, Phys. Rev. B **54**, 17 954 (1996).

[13] K. Wakabayashi, M. Fujita, H. Ajiki, and M. Sigrist, Phys. Rev. B **59**, 8271 (1999).

[14] R. C. Teitelbaum, S. L. Ruby, and T. J. Marks, J. Am. Chem. Soc. **101**, 7569 (1979).

[15] L. Grigorian, K. A. Williams, S. Fang, G. U. Sumanasekera, A. L. Loper, E. C. Dickey, S. J. Penneycook, and P. C. Eklund, Phys. Rev. Lett. **80**, 5560 (1998).

[16] Y. Shibayama, H. Sato, T. Enoki, X. X. Bi, M. S. Dresselhaus, and M. Endo, J. Phys. Soc. Jpn. **69**, 754 (2000).

[17] M. S. Dresselhaus and G. Dresselhaus, Adv. Phys. **30**, 139 (1981).

[18] B. L. V. Prasad, H. Sato, T. Enoki, Y. Hishiyama, and Y. Kaburagi, Mol. Cryst. Liq. Cryst. **340**, 793 (2000).

[19] S. Y. Leung, C. Underhill, G. Dresselhaus, T. Krapchev, R. Ogilive, and M. S. Dresselhaus, Solid State Commun. **32**, 635 (1979).

[20] *International Tables for X-ray Crystallography* (Kynoch, Birmingham, England, 1974), Vol. III, p. 201.

[21] R. J. Nemanich and S. A. Solin, Phys. Rev. B **20**, 392 (1979).

[22] P. C. Eklund and K. R. Subbaswamy, Phys. Rev. B **20**, 5157 (1979).

[23] A. M. Rao, P. C. Eklund, S. Bandow, A. Thess, and R. E. Smalley, Nature (London) **388**, 257 (1997).

[24] P. C. Eklund, G. Dresselhaus, M. S. Dresselhaus, and J. E. Fischer, Phys. Rev. B **16**, 3330 (1977).

[25] M. Murata and H. Suematsu, J. Phys. Soc. Jpn. **51**, 1337 (1982).

[26] B. L. V. Prasad, H. Sato, T. Enoki, Y. Hishiyama, and Y. Kaburagi (unpublished).

[27] S. K. Khanna, E. R. Falardeau, A. J. Heeger, and J. E. Fischer, Solid State Commun. **25**, 1059 (1978).

[28] S. A. Safran, in *Solid State Physics*, edited by H. Ehrenreich and D. Turnbull (Academic, New York, 1987), Vol. 40, p. 183.

[29] G. Kirczenow, Phys. Rev. Lett. **52**, 437 (1984).

[30] G. Kirczenow, Phys. Rev. B **31**, 5376 (1985).

[31] P. C. Eklund, E. T. Arakawa, G. D. Mahan, J. L. Zarestky, and W. A. Kamitakahara, Synth. Met. **12**, 97 (1985).

[32] A. M. Rao (unpublished).

[33] C. T. Chan, K. M. Ho, and W. A. Kamitakahara, Phys. Rev. B **36**, 3499 (1987).

[34] J. W. McClure, Phys. Rev. **119**, 606 (1960).

[35] S. A. Safran and F. J. DiSalvo, Phys. Rev. B **20**, 4889 (1979).

[36] S. Ikehata, H. Suematsu and S. Tanuma, Solid State Commun. **50**, 375 (1984).

[37] H. Suematsu, S. Tanuma and K. Higuchi, Physica B **99B**, 420 (1980).

[38] A. S. Kotosonov, Pis'ma Zh. Eksp. Teor. Fiz. **43**, 30 (1986) [JETP Lett. **43**, 37 (1986)].

[39] J. Blinowski, N. H. Hau, C. Rigaux, J. P. Vieren, R. L. Toullec, G. Furdin, A. Herold, and J. Melin, J. Phys. (Paris) **41**, 47 (1980).

[40] R. Saito, Ph.D. thesis, University of Tokyo, 1984.

[41] T. Inoshita, K. Nakao, and H. Kamimura, J. Phys. Soc. Jpn. **43**, 1237 (1977).

[42] N. Ganguly and K. S. Krishnan, Proc. R. Soc. London, Ser. A **177**, 168 (1941).

[43] G. Wagoner, Phys. Rev. **118**, 647 (1960).